where

$$I(z)=\int_{-\infty}^{\infty}-\frac{da}{\sqrt{2\pi}}\exp\left[-\tfrac{1}{2}a^2-\frac{1}{a^4}\frac{g^2}{2\pi}\frac{K_0^2(mb)}{Y_c}(1-z^2)\right.$$
$$\left.-\frac{i}{a}\frac{g^2K_0(mb)\sqrt{2}}{2\pi\sqrt{Y_c}}(1-z)\right]. \quad (14)$$

From (13) and (14), one sees that

$$\sigma_{\rm tot}=2\int d^2b(1-{\rm Re}e^{i\chi}), \quad (15)$$

$$\sigma_{\rm el}=\tfrac{1}{2}\sigma_{\rm tot}-\int d^2b\,\frac{1}{2\sqrt{\pi}}\,g^2K_0(mb)\frac{1}{\sqrt{Y_c}}, \quad (16)$$

showing that, asymptotically,

$$\tfrac{1}{2}\sigma_{\rm tot}\sim\sigma_{\rm el}\sim\sigma_{\rm inel}.$$

Also, from (14) one finds at $z=1$ a singularity of $I(z)$ of type $e^{a(1-z)^{1/2}}$, and hence one cannot calculate the multiplicity $\langle n\rangle$ without inserting appropriate cutoffs to ensure energy conservation.[5]

In summary: In this simple model, it is seen that the asymptotic approach to $\sigma_{\rm tot}(pp)$ is from below. In the absence of explicit energy conservation for inelastic processes, a singularity in the fugacity plane at $z=1$ appears in $\sigma_{\rm tot}(z)$.

The author thanks Professor H. M. Fried for guidance and discussions throughout this work.

*Work supported in part by the U. S. Atomic Energy Commission.

[1]The question concerns the sign of the two-Reggeon cut contribution to a cross section approaching its asymptotic limit from above or below. For arguments leading to a positive sign, see, for example, G. F. Chew, Phys. Rev. D 7, 934 (1973); H. D. I. Abarbanel, *ibid.* 6, 2788 (1972). For a negative sign, see, for example, R. Blankenbecler, SLAC Report No. SLAC-TN-72-13, 1972 (unpublished). See also A. R. White, CERN Report No. TH-1646, 1973 (unpublished); V. N. Gribov, Zh. Eksp. Teor. Fiz. 53, 654 (1967) [Sov. Phys.—JETP 26, 414 (1968)].

[2]R. Blankenbecler and H. M. Fried, Phys. Rev. D 8, 678 (1973). See also H. M. Fried, *Functional Methods and Models in Quantum Field Theory* (MIT Press, Cambridge, Mass., 1972), Chap. 10.

[3]H. M. Fried, Phys. Rev. D 6, 3562 (1972).

[4]Reference 2, Chap. 9.

[5]For example, see the method used by H. Cheng and T. T. Wu, Harvard Univ. report, 1973 (unpublished).

PHYSICAL REVIEW D VOLUME 8, NUMBER 9 1 NOVEMBER 1973

Anomalous Magnetic Moment of the Electron

M. J. Levine*
Physics Department, Carnegie-Mellon University, Pittsburgh, Pennsylvania 51213

Jon Wright†
Physics Department, University of Illinois, Urbana, Illinois 61801

(Received 8 June 1973)

We present detailed results of our previously published calculation of the sixth-order magnetic moment of the electron. The numerical accuracy has been improved, resulting in a value $a_e=\frac{1}{2}\alpha/\pi-0.32847\,(\alpha/\pi)^2+1.21\,(\alpha/\pi)^3$, which is in reasonable agreement with the latest experimental result.

I. INTRODUCTION

In a previous paper[1,2] we reported on a numerical calculation of the sixth-order anomalous magnetic moment of the electron. In this paper we present detailed results and a discussion of our method. At present there appears to be reasonable agreement between theoretical calculations and experiment. In addition to the actual calculation we present a new method of handling infrared singularities in Feynman graphs in numerical calculations.

In Sec. II we summarize past $g-2$ calculations and present our results for individual graphs. We also compare theory and experiment there. In Sec. III we briefly review the method of reducing the momentum-space integrals to parametric integrals. In Sec. IV we discuss the introduction of ultraviolet and infrared counterterms. We made no attempt to make use of Ward identities and we just evaluated each diagram in "cookbook" fashion. In Sec. V we discuss the actual numerical integration.

The results presented in Sec. II suggest that a

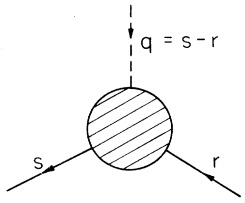

FIG. 1. General fermion-photon vertex graph.

slight improvement in the experiment and an improvement in the theoretical calculation will give a very precise value for α, assuming the validity of quantum electrodynamics (QED). It is hoped that the detailed results presented here will enable others to compare their calculations and isolate any discrepancies. It is relatively easy to improve the accuracy for an individual graph if such discrepancies are discovered. Since there are no other published numbers for most individual graphs, these results should help those doing analytical calculations. Finally, the method of treating infrared divergences should prove applicable elsewhere.

II. PRESENT STATUS OF $(g-2)_e$

The amplitude for the vertex function of Fig. 1 may be written

$$-ie\bar{u}(s)\left[F_1(q^2)\gamma_\mu + \frac{F_2(q^2)}{2m} i\sigma_{\mu\nu}q_\nu\right]u(r), \qquad (2.1)$$

where F_1 and F_2 are the charge and moment form factors. The anomalous moment is obtained by extracting

$$a \equiv F_2(0) = \tfrac{1}{2}(g-2)$$
$$= \frac{1}{2}\frac{\alpha}{\pi} + a_4\left(\frac{\alpha}{\pi}\right)^2 + a_6\left(\frac{\alpha}{\pi}\right)^3 + \cdots \qquad (2.2)$$

from the perturbation theory graphs. The second-[3] and fourth-order[4,5] contributions have been calculated by several groups. The corresponding graphs are shown in Figs. 2 and 3. The results for the fourth order[4,5] are summarized in Table I for completeness. The sixth-order graphs are shown in Figs. 4 and 5. In Table II we summarize the results of the various calculations[6-13] of graphs 29–40. Graphs 29–31 and 36–37 are known analytically. In Table III we summarize the results of our calculations for graphs 1–28. All of these graphs are calculated in the Feynman gauge. Independent numerical results for graphs 1–3 (see Ref. 14) and analytic results for graphs 2, 11, 13, 21, 23, and 24 (see Ref. 15) are also included. Unfortunately, the analytic results are for graphs which are easy to do numerically. It is comforting to see that our error estimates are conservative, as the actual error is less than one-third of our estimated error. In Table IV we have collected sums of certain subsets of graphs 1–28. We use the following set of numbers in evaluating a_6:

Graphs (1–28) 0.943 ± 0.06,
(29–31) 0.05429,
(32–38) -0.154 ± 0.005,
(39–40) 0.370 ± 0.013,
$a_6 = (1.21 \pm 0.07)$.

Kinoshita and Cvitanovic[16] have also evaluated graphs 1–28 and they obtain a slightly higher result for a_6, a_6 (1–28) $= 1.02 \pm 0.04$ and $a_6 = 1.29$

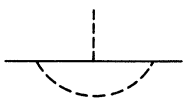

FIG. 2. Second-order fermion-photon vertex graph. Those graphs which vanish after mass-shell renormalization are not included.

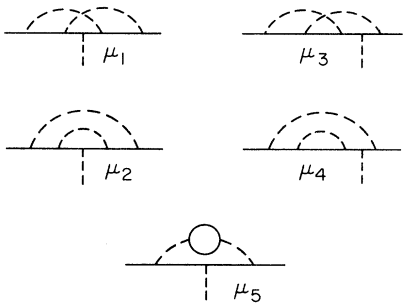

FIG. 3. Topologically unique fourth-order fermion-photon vertex graphs. Those graphs which vanish after mass-shell renormalization are excluded.

TABLE I. Values for fourth-order graphs shown in Fig. 3 plus their mirror images. $a_4 = -0.328\,479\,4$.

Graph	a_4	Coeff. of $\ln\lambda^2$
1	$\frac{1}{6} + \frac{13}{36}\pi^2 + \frac{5}{4}\zeta(3) - \frac{5}{6}\pi^2\ln 2$ $(=-0.467=\mu_1)$	
2	$\frac{11}{48} + \frac{1}{18}\pi^2$ $(=0.778=\mu_2)$	
3	$-\frac{67}{24} + \frac{1}{18}\pi^2 - \frac{1}{2}\zeta(3) + \frac{1}{3}\pi^2\ln 2$ $(=-0.564=\mu_3)$	$-\frac{1}{2}$
4	$\frac{11}{24} - \frac{1}{18}\pi^2$ $(=-0.090=\mu_4)$	$\frac{1}{2}$
5	$\frac{119}{36} - \frac{1}{3}\pi^2 = 0.016$	

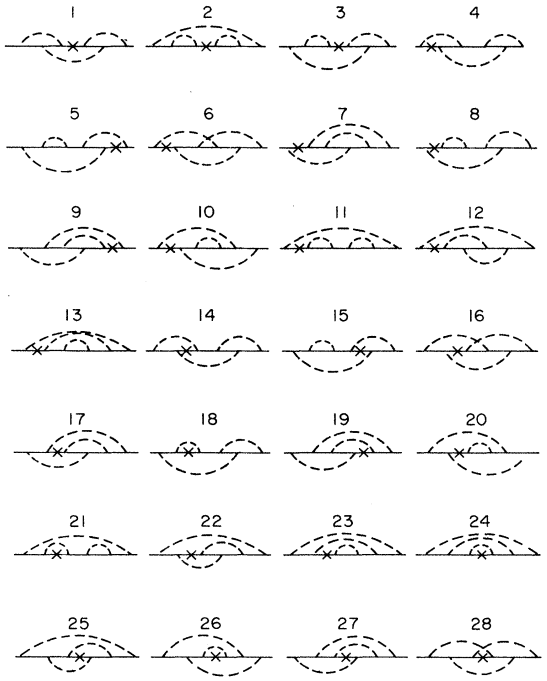

FIG. 4. Sixth-order vertex graphs without closed fermion loops.

± 0.06. Carroll and Yao[17] have also reported a calculation with the result $a_6\,(1\text{–}28) = 0.74 \pm 0.06$. Using $\alpha^{-1} = 137.03\,608\ (\pm 26)$, we obtain

$$a^{\text{th}} = (1\,159\,651.9 \pm 2.5) \times 10^{-9}.$$

The uncertainty in a^{th} arises from uncertainty in $\alpha(2.2)$ and in the numerical a_6 result (1.0). The latest experimental value[18] is

$$a^{\text{exp}} = (1\,159\,656.7 \pm 3.5) \times 10^{-9},$$

which is in fair agreement with theory. We can use the experiment to obtain a value for α:

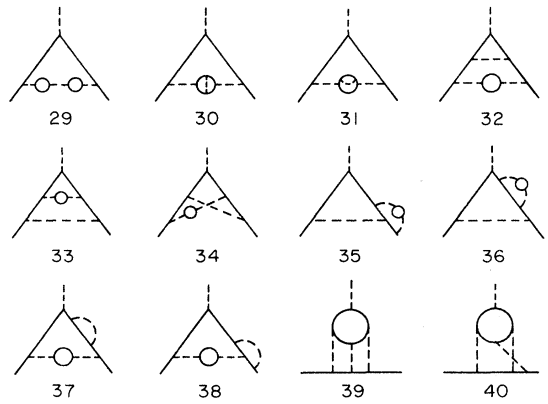

FIG. 5. Sixth-order vertex graphs with closed fermion loops.

$$\alpha^{-1} = 137.035\,51 \pm 54.$$

Of this error, 44 is from a^{exp} and 10 from a^{th} (the discrepancy between our a_6 and Ref. 16 corresponds to an error of 11). Thus, a modest increase in both the experimental and the theoretical accuracy will give an independent value for α. The value of a_6 calculated by Kinoshita and Cvitanovic[16] gives

$$\alpha^{-1} = 137.035\,63.$$

For further discussion on the present status of QED, see Refs. 19, 20, and 21. For an alternative method of calculating these graphs, see Ref. 22.

III. REDUCTION TO QUADRATURES

While the evaluation of vertex graphs is a straightforward task, the large number of graphs and their high order has led us to choose a very systematic procedure for their evaluation. This procedure is also well suited to implementation on a computer. The general scheme is that described by Chisholm.[23] We briefly review it.

TABLE II. Results for graphs shown in Fig. 5 plus their mirror images.

Graph	a_6	
29	0.002 558 5	Ref. 9
	0.002 56 (15)	Ref. 7
30–31	0.052 870	Ref. 9
	0.052 (2)	Ref. 7
29–31	0.055 46 (6)	Ref. 6
32–33	0.0522 (10)	Ref. 7
	0.0532 (4)	Ref. 6
34	−0.0031 (10)	Ref. 7
	−0.0032 (3)	Ref. 6
35	0.0274 (5)	Ref. 7
	0.0273 (3)	Ref. 6
36	−0.1151 (9)	Ref. 7
	−0.1161 (14)	Ref. 6
	−0.115 446 4	Ref. 11
37	−0.0653 (3)	Ref. 7
	−0.064 (3)	Ref. 6
	−0.066 467	Ref. 12
38	−0.0474 (20)	Ref. 7
	−0.051 (3)	Ref. 6
32–38 [a]	−0.1528 (25)	Ref. 7
	−0.1556 (31)	Ref. 6
39–40	0.36 (4)	Ref. 8
	0.366 (10)	Ref. 13
	0.37 (1)	Ref. 10

[a] Includes analytic result for 36, 37. The errors in the other graphs were assumed to be random.

TABLE III. Coefficient of $(\alpha/\pi)^3$ for a_6. The values shown are for the graph plus its mirror image (if any). Graphs marked a were calculated in pairs, i.e., (16+28) and (19+27). Consequently the sum is more accurate than individual terms. The smallest error is for the sum. The μ's are finite parts of fourth-order graphs—see Table I.

Graph	a_6		$\frac{1}{2}\ln\lambda^2$	$(\ln\lambda^2)^2$
1	−2.746 (7)		$-\mu_3$	$\frac{1}{8}$
	−2.728 (16)	Ref. 14		
2	−3.374 (2)		μ_4	$\frac{1}{8}$
	−3.332 (11)	Ref. 14		
	−3.374 31	Ref. 15		
3	6.541 (13)		$\mu_3-\mu_4$	$-\frac{1}{4}$
	6.538 (12)	Ref. 14		
4	−1.211 (13)		$-\mu_3$	$\frac{1}{8}$
5	0.832 (13)		μ_3	$-\frac{1}{8}$
6	2.581 (13)		1	
7	−2.664 (20)		$-\mu_3-1$	$\frac{1}{8}$
8	−0.083 (6)		$\mu_3-\mu_4$	$-\frac{1}{4}$
9	0.625 (6)		$-\mu_3$	$+\frac{1}{8}$
10	0.795 (6)		μ_3	$-\frac{1}{8}$
11	−2.463 (2)		$2\mu_4$	$\frac{1}{4}$
	−2.463 23	Ref. 15		
12	−0.123 (20)		$-2\mu_4-1$	$-\frac{1}{4}$
13	2.270 (10)		μ_4+1	$\frac{1}{8}$
	2.264 95	Ref. 15		
14	5.515 (25)		$-2\mu_1$	
15	−3.951 (40)		$2\mu_1$	
16 [a]	−1.763 (20)			
17	0.613 (13)		$-2\mu_1$	
18	−4.201 (13)		$-(\mu_3+2\mu_2)$	$\frac{1}{8}$
19 [a]	−0.330 (13)			
20	−0.153 (6)		$2\mu_1$	
21	5.308 (2)		$2\mu_2-\mu_4$	$-\frac{1}{8}$
	5.308 08	Ref. 15		
22	−0.005 (20)		$\mu_3-2\mu_2$	$-\frac{1}{8}$
23	−1.512 (6)		$\mu_4+2\mu_2$	$+\frac{1}{8}$
	−1.509 70	Ref. 15		
24	1.789 (2)			
	1.790 28	Ref. 15		
	1.777 (13)	Ref. 22		
25	−1.286 (13)		$\mu_1+\frac{1}{2}$	
26	−1.888 (6)		$-\mu_1-\frac{1}{2}$	
27 [a]	1.854 (13)			
28 [a]	−0.021 (100)			

A general term with which we must deal is of the form

$$\int dk_1\cdots\bar{u}(s)\gamma_\alpha(\not l_1+\not p_1-m)^{-1}\gamma_\beta(\not l_2+\not p_2-m)^{-1}\times\cdots\gamma_\mu\cdots u(r)\,k_1^{-2}k_2^{-2}\cdots,$$

where $\bar{u}(s)$ and $u(r)$ are final and initial spinors, $\gamma_\alpha\cdots\gamma_\alpha$ are internal photon vertices, γ_μ is the external field vertex, $(\not l_i+\not p_i-m)^{-1}$ is a fermion propagator, and k_j^{-2} is a photon propagator. p_i is an external, constant four-momentum associated with the ith fermion line. $p_i=r$ or s depending upon the line. $l_i=\sum_j a_{ij}k_j$, $i=1,\ldots,6$; $a_{ij}=\pm1,0$. The fermion propagators are rationalized and the denominators are combined by introducing Feynman parameters using

$$(A_1A_2\cdots A_n)^{-1}=(n-1)!\int dx_1\cdots dx_n\times\delta(1-x_1-\cdots-x_n)D^{-n},$$

where $D=\sum_i x_iA_i$. We now have a denominator of the form $D=\sum_{ij}A_{ij}k_i\cdot k_j+2\sum_i B_i\cdot k_i+C$, where $A_{ij}=\sum_k a_{ki}a_{kj}x_k$, $B_i=\sum_j a_{ji}p_jx_j$, $C=\sum_i(p_i^2-m_i^2)x_i$. If we now perform translations and rotations in k space to diagonalize the denominator and bring it to the form $D=\sum_i A'_{ii}k_i'^2+C'$, the propagator numerators will assume the form $(\not l'_i+N_i)$, where $N_i=(\frac{1}{2}S_i\not p+\frac{1}{2}D_i\not q+m)$, $p=r+s$, and $q=s-r$. The S_i and D_i are functions of the x_j only and l'_i is a linear function of k'_j with coefficients depending upon the x_j. Since the denominator is now diagonalized and even in the k'_i, only numerator terms even in k'_i survive the symmetric dk' integrations. These integrations may now be done. We note that

$$\int k'_{i\alpha}k'_{i\beta}\frac{dk'}{D^n}=\tfrac{1}{4}g_{\alpha\beta}\int k_i'^2\frac{dk'}{D^n}.$$

TABLE IV. Sums of graphs corresponding to fermion self-energy graphs (upper) and to gauge-invariant sets (lower).

Graphs	a_6
1, 4, 14	1.559
6, 16, 28	0.798
2, 11, 21	−0.530
13, 23, 24	2.547
12, 22, 25	−1.414
10, 20, 26	−1.249
7, 9, 17, 19, 27	0.097
3, 5, 8, 15, 18	−0.867
1–3	0.421
4–13	0.558
14–23	−0.483
24–28	0.445

As a result of this kind of integration in addition to terms where each fermion-propagator numerator is replaced by N_i, there will be terms having $\gamma_\alpha \cdots \gamma_\alpha$ in place of two numerators while all other numerators are replaced by N_i. These "pairing" terms are of the form $\gamma_\alpha \cdots \gamma_\alpha \cdot V_{ij}$, where V_{ij} is a function of the x_j. In fact we must consider all possible terms having $0, 1, \ldots, (\frac{1}{2}n)$ pairings. While it is possible to absorb the p_i term in N_i into S_i and D_i, we segregate it because of the way in which it enters into infrared-divergent terms.

The S_i, D_i, and V_{ij} are easily found in the following way: Restarting from the initial expression, let each p_i be a formal, unique variable. We will give it its actual value much later. We replace $(\not{l}_i + \not{p}_i)$ in the propagator numerators by ϕ_i.

$$O_{i\alpha} = \int_{m_i^2}^{\infty} \frac{d\sigma_i}{2} \left(\frac{\partial}{\partial p_{i\alpha}} \right),$$

where σ_i is a dummy name for the square of the mass of the ith electron. This removes all explicit numerator dependence upon the integration momenta k. After parametrization the dk integrations can be performed using $\int dk_1 \cdots dk_n / D^n = U^{n-2m-2}/W^{n-2m}$, where U is the determinant of the A_{ij} and

$$W = \begin{vmatrix} A_{ij} & B_i \\ B_j & C \end{vmatrix}.$$

The operator O_i acts upon the B_i and C in W: $O_i W^{-n} = (T_i/U + p_i) W^{-n}$. The next operator, O_j, can act on W or on $(T_i/U + p_i)$ to give

$$O_{i\alpha} O_{j\beta} W^{-n} = \left(\frac{T_i}{U} + p_i \right)_\alpha \left(\frac{T_j}{U} + p_j \right)_\beta W^{-n} - \frac{T_{ij} g_{\alpha\beta}}{2(n-1) U^2 W^{n-1}}.$$

W is quadratic in the p_i, T_i is linear, and T_{ij} is independent of the p_i. There are no worse than "pairing" terms, although all possible pairing combinations will arise. When calculating a graph in this way, it is necessary to include renormalization subtraction terms at this stage—otherwise the operations above are not always well defined.

We may now let $p_i = r$ or s in W, T_i, T_{ij}. Going to the limit $q^2 = 0$, $r^2 = s^2 = r \cdot s = m^2 = 1$ we find that W, T_{ij} now depend only on the x_i, while T_i is linear in r and s with coefficients depending only on the x_i. We can now identify $T_i/U = \frac{1}{2} S_i\, p + \frac{1}{2} D_i\, q$; $-T_{ij}/[2(n-1)U^2] = V_{ij}$; $T_{hi}\, T_{jk} W^2/[2(n-1) \times (n-2) U^2] = V_{hi}\, V_{jk}$; etc. The W can be written by inspection for any graph and U, S, D, V are just combinations of minors of W and the x_i.

Done in this way each sixth-order graph produces 8671 terms. There are 4^6 nonpairing terms, 15×4^4 single-pairing terms, 45×4^2 double-pairing terms, and 15 triple-pairing terms. Many of these terms quickly drop from the calculation and many others can be combined to provide simplification. However, initial generation of terms in this manner greatly facilitates the calculation by systematizing it.

Finally, we must extract the $F_2(0)$ part of a graph. For renormalization purposes we will sometimes require the $F_1(0)$ part. The usual way to do this is to multiply the expression between spinors by a projection operator and take traces.[8] However, since the $\int dk$ has been done, it is much easier to extract the contribution to either form factor directly. At this stage each of the terms has a product of the factors v ($v = \not{p}, \not{q}, \not{r}, \not{s}, m$), $\gamma_\alpha \cdots \gamma_\alpha$, γ_μ between spinors. After the usual $\gamma_\alpha \cdots \gamma_\alpha$ identities are utilized, each term is of the form $\bar{u}(s) \cdots \gamma_\mu \cdots u(r)$, where "$\cdots$" denotes some product of the v's. The vertex function (2.1) can be rewritten as

$$-ie\bar{u}(s) \left[(F_1 + F_2)\gamma_\mu - F_2 \left(\frac{r+s}{2m} \right)_\mu \right] u(r).$$

In principle we should include a term $q_\mu F_3(q^2)$, but this term vanishes for the sum of a graph plus its mirror image. In addition the projection technique we use is orthogonal to F_3. Letting $L(A, B) = A\not{r} + B$ and $R(C, D) = C\not{s} + D$ so that $L(0, 1) = R(0, 1) = 1$, we can write a term as $\bar{u}(s) L(0, 1) \cdots \gamma_\mu \cdots \times R(0, 1) u(r)$. Using the Dirac equation with $m = 1$ and $q^2 = 0$, we see that $\bar{u}(s) L(A, B) v = \bar{u}(s) L(A', B')$, where A' and B' are some linear combination of A and B which depends upon which v we have. Similar relations hold for $vR(C, D)u(r)$. We use these relations to reduce the expression to $\bar{u}(s) L(A, B) \gamma_\mu R(C, D) u(r)$, for which $F_1(0) = (A + B) \times (C + D)$ and for which $F_2(0) = A(C + D) + (A + B)C$. This allows us to readily extract the contribution to $F_{1,2}(0)$ for each of the terms for each graph. The expression for the contribution to $F_{1,2}(0)$ from a graph is now simply in terms of W, U, S_i, D_i, and V_{ij}, all of which are functions only of the Feynman parameters over which we must integrate. It is thus reduced to quadratures. The algebra was done by machine using a program written by Levine.[24]

IV. ULTRAVIOLET AND INFRARED SINGULARITIES

The diagrammatic expansion and the procedures we have outlined above are plagued by the existence of nonintegrable singularities in the integrands. In fact, because of these singularities, many of the operations we have performed above are only formal. The singularities are of two

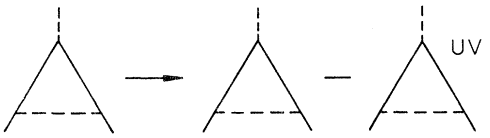

FIG. 6. Second-order vertex insertion and the renormalizing UV counterterm.

types: the ultraviolet (UV) divergences associated with the short-distance behavior of the theory and the infrared (IR) divergences associated with the long-range behavior of the photon propagator. These singularities are well understood. Analytically, they are readily handled by regularization using UV and IR cutoffs. For example, the substitution

$$\frac{1}{k^2} \to \frac{1}{k^2-\lambda^2} - \frac{1}{k^2-\Lambda^2}, \quad \lambda^2 \text{ small}, \ \Lambda^2 \text{ large}$$

produces finite, cutoff-dependent quantities. Then, for this problem, renormalization and cancellations between graphs produce a result which is finite as $\lambda^2 \to 0$, $\Lambda^2 \to \infty$.

The momentum-space expressions for the diagrams have nonintegrable singularities at $k=0,\infty$. Although we have formally performed the $\int dk$, those divergences now appear in parameter space. When certain of the $x_i \to 0$, W vanishes in such a way that the $\int dx$ is divergent. We are obliged to integrate our functions numerically. In that case it is undesirable to introduce any explicit cutoffs and either hope for approximate numerical cancellations of cutoff-dependent parts between graphs or to evaluate the functions for many values of the cutoff parameters and do an extrapolation to the appropriate limit. Instead, we have handled these problems in a way which produced integrable, cutoff-independent functions in both momentum space and Feynman parameter space.

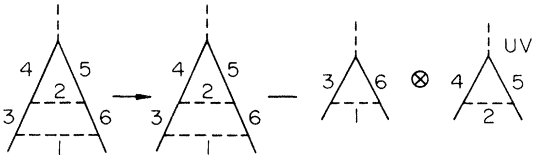

FIG. 7. A fourth-order vertex function before and after the introduction of renormalizing vertex UV insertions. The symbol ⊗ means multiplication.

For the UV divergences we have introduced the usual renormalization counterterms.[23] The vertex function requires one subtraction

$$\Lambda_\mu(p',p) \to \Lambda^r_\mu(p',p) = \Lambda_\mu(p',p) - \Lambda_\mu(p_0,p_0),$$

where p_0 is a mass-shell momentum. This may be represented graphically for the second-order vertex as shown in Fig. 6. In Fig. 7 we draw the main and UV counterterm for the fourth-order ladder graph. Here we ignore the over-all subtraction which does not contribute to the magnetic moment. Although we may consider the counterterm numerator to be factored into two second-order pieces, we parametrize the counterterm denominator as we parametrized the main-term denominator:

$$W_M = W_{\text{main}} = \begin{vmatrix} x_1+x_2+x_3+x_4+x_5 & x_2+x_3 & x_1+x_2+x_3+x_4 \\ x_2+x_3 & x_2+x_3+x_6 & x_2+x_3 \\ x_1+x_2+x_3+x_4 & x_2+x_3 & 0 \end{vmatrix},$$

$$W_c = W_{\text{counter}} = \begin{vmatrix} x_1+x_4+x_5 & 0 & x_1+x_4 \\ 0 & x_2+x_3+x_6 & x_2+x_3 \\ x_1+x_4 & x_2+x_3 & 0 \end{vmatrix}.$$

For the numerator of the counter-graph we use the S, D, V's obtained from W_c. In this way we produce a counterterm which when subtracted from the main term leaves a function free from UV divergences point by point in parameter space. We treat the electron self-energy insertions in a similar manner:

$$S(p) \to S^r(p) = S(p) - S(p_0) - (\not{p}-m)\left[\frac{\partial S(p)}{\partial p}\right]_{p_0}.$$

In Fig. 8 we give an example for a fourth-order graph. The bar on the electron line represents the operator 1 (i.e., there is a propagator on either side of the bar).

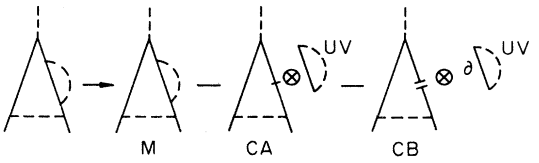

FIG. 8. A fourth-order vertex graph before and after the introduction of renormalizing electron propagator UV insertions. The electron line with the double bar denotes the factors $(\not{p}-m)^{-1}$ $(\not{p}-m)$ $(\not{p}-m)^{-1}$. To keep point-by-point parameter-space cancellation, the numerator and denominator factors cannot be canceled to give 1. The single bar separates the line into two propagators, $(\not{p}-m)^{-1}\cdot(\not{p}-m)^{-1}$.

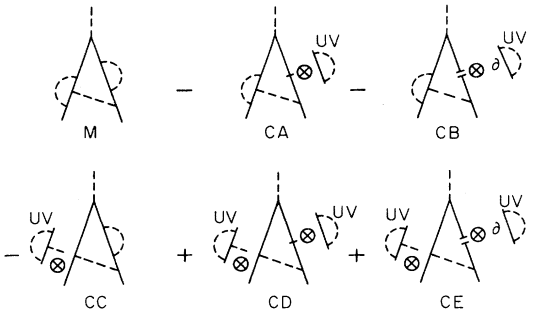

FIG. 9. Sixth-order graph 3 with UV counterterms. Both vertex and electron propagator renormalizations are included. CA and CB have the same denominator as do CD and CE.

ther side of the bar). The sixth-order graph of Fig. 9 (graph 3) contains both vertex and propagator insertions. Note that while there are a total of six graphs in this case, there are only four different W's. Those graphs having the same characteristic denominator are grouped together. Using this procedure, all UV divergences are removed and the necessary renormalization is performed.

We have used an analogous procedure to handle the IR divergences.[1,2] It is based upon the factorization property used to show general, analytical cancellation of IR divergences.[25] In momentum space the IR divergences arise when some photon momenta in a graph go to zero. If, as in Fig. 10, a vertex graph (C) can be written as a combination of a vertex graph (A) and a proper two-particle scattering graph (B), then when all photon momenta in B vanish (k_B), we have an IR divergence. If we are interested in $F_2(0)$, then A must be of higher than first order. For $F_1(0)$, the cases where A is the bare vertex must also be considered. Such situations arise in main and UV counter graphs and in the second subtraction terms for electron-propagator renormalizations. The latter are very like vertex graphs as seen from Ward's identity. While these two quantities are formally identical, they are divergent and great care must be taken in handling them.

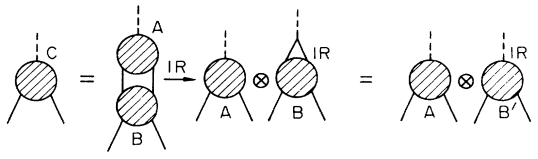

FIG. 10. General fermion vertex graph (C) separated into a vertex (A) and scattering (B) graph. In the IR limit, $k_B \to 0$, this factors into a vertex graph (A) multiplied by the IR limit of the vertex graph (B′) corresponding to the scattering graph.

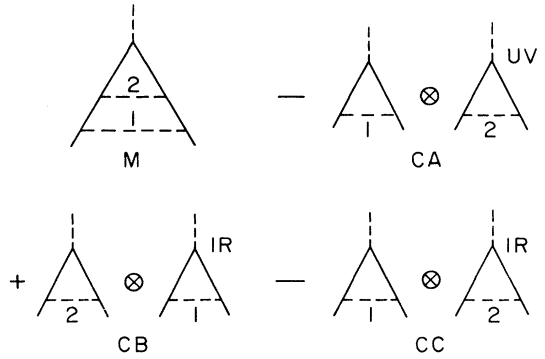

FIG. 11. Fourth-order ladder vertex graph with UV counterterm (CA) and IR counterterms (CB) and (CC). (M − CA) is UV-convergent. (M − CB) and (CA − CC) are IR-convergent. CB = CC so that the sum of the IR counterterms is zero.

In the IR limit, $k_B \to 0$, the fermion lines joining A and B go to the mass shell and the graph factors. The resultant expression for the B part of the graph is the IR limit of the $F_1(0)$ part of the corresponding vertex graph (B′). We represent it graphically as shown in Fig. 10. The IR limit involves deleting all references to the k_B in A and replacing the fermion propagators in B, $1/(\not{p}_i + \not{k}_B - m)$, with the expressions $(\not{p}_i + m)/[(p_i + k_B)^2 - m^2]$. In these expressions all numerator terms involving the k_B are missing. Both the V_{ij} or pairing terms and the S_i and D_i parts of N_i disappear. It is towards this eventuality that we have segregated the p_i term in each N_i.

As an example, consider the fourth-order ladder graph. In Fig. 11 we have drawn the main graph M and UV counterterm CA, and subtracted (CB) and added (CC) the IR limits of graphs M and CA, respectively. If we parametrize the subtracted counterterm (CB) in parallel with the main graph, as we did for the UV counterterms, the difference

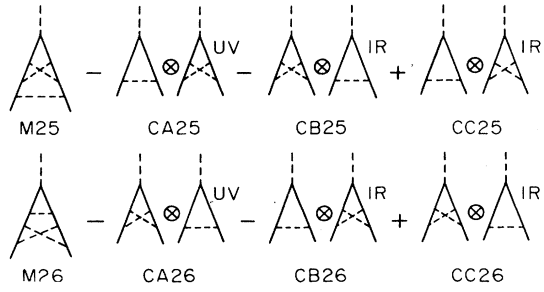

FIG. 12. Main, UV, and IR counterterms for sixth-order graphs 25 and 26. (M25 − CA25) and (M26 − CA26) are UV-convergent. (M25 − CB25), (CA25 − CC25), (M26 − CB26), and (CA26 and CC26) are IR-convergent. CB25 = CC26 and CC25 = CB26 so that the total added IR counterterm is zero.

(M − CB) will be IR-divergence-free in k space and point-by-point integrable in parameter space. However, unlike the UV case, this counterterm has no physical meaning and must finally be reincluded. If desired, this may be done analytically or numerically to obtain a term like $(a+b\ln\lambda^2)$ in the limit $\lambda^2 \to 0$. This will be comparatively easy since we have now factored the graph into lower-order pieces.

The UV counterterm (CA) for this graph is also IR-divergent. The necessary IR counterterm (CC) is, in this case, the same as for the main graph but of opposite sign. The only difference between the two IR counterterms is in the labeling of some variables of integration. For the graphs in Fig. 11 the UV divergences cancel between M and CA, while the IR divergences cancel between M and CB and between CA and CB. CB and CC cancel identically after integration. There is no need to calculate even lower-order IR-divergent terms for this graph.

In general such IR divergence cancellations occur between graphs rather than within a single graph. In that case no explicit IR-divergent terms need be calculated unless one wants a cutoff-dependent result for a single graph. For $F_2(0)$ there are subsets of graphs that are gauge-invariant corresponding to sets that have the same number of virtual photon lines crossing the external field vertex. The IR counterterms cancel within each subset. We have, in addition, evaluated those fourth- and second-order IR divergences needed to obtain an explicit IR cutoff-dependent value for each of our sixth-order graphs. As a final example consider the main and counterterms for diagrams 25 and 26 as shown in Fig. 12. In this case all IR counterterms cancel between the two graphs.

The situation is slightly more complicated for $F_2(q^2)$ for $q^2 \neq 0$ or for $F_1(q^2)$. The same technique described above will work; however, the infrared counterterms will have to be evaluated. Fortunately, they are always of lower order. They will also have to be calculated for the case when the two fermion legs have different momentum. There should be no trouble in practice in generalizing the technique to these cases.

TABLE V. Values for fourth-order counterterms shown in Fig. 11. A corresponds to μ_1, B to μ_2, C to μ_3, and D to μ_4.

$$A = -0.9675\ (2) - \tfrac{1}{2}\ln\lambda^2$$
$$B = 2.701\,11\ (5) + \tfrac{1}{2}\ln\lambda^2 + \tfrac{1}{8}(\ln\lambda^2)^2$$
$$C = 0.7336\ (3) + \tfrac{1}{8}(\ln\lambda^2)^2$$
$$D = -1.7898\ (1) + \tfrac{1}{4}\ln\lambda^2 + \tfrac{1}{8}(\ln\lambda^2)^2$$

While these procedures produce a great many counterterms, they are very readily found and easily reduced to parameter-space expressions using the same techniques as are needed for the main graphs. The resultant parameter-space functions are everywhere integrable and no divergent expressions need to be evaluated. Explicit cutoffs are avoided at all stages. For the fourth order these procedures produce the usual results.

Alternatively one can try to separate the IR divergences in parameter space. In our opinion this is considerably less transparent than the introduction of IR counterterms in momentum space, which is very simple and straightforward.

There are four irreducible fourth-order infrared counterterms needed. They are the same graphs as $\mu_1 - \mu_4$ in Fig. 3 with special rules for evaluation. The graphs are evaluated with all photon momenta deleted from numerators of propagators with the exception of D, where we found it convenient to keep the photon momentum for the self-energy insertion, in which case the renormalization terms are also included.

The values for these graphs are given in Table V. In Table VI we list the sixth-order IR counterterms necessary for each graph.

V. NUMERICAL INTEGRATION AND ERRORS

Having produced integrable expressions in parameter space we must now integrate them. Certain trivial integrations can be done analytically leaving 5-, 6-, and 7-dimensional integrals to be done numerically in sixth order. We have used both the adaptive Monte-Carlo technique of Sheppey[26] and simple Legendre-Gaussian quadrature in each variable after mapping the simplex $\sum x_i = 1$ onto a hypercube and applying various transformations mapping (0, 1) onto (0, 1) with Jacobian $x^a(1-x)^b$. These mappings are used to control the integrable but singular behavior of the integrands at the endpoints. The high-precision runs are done with the Gaussion points. Convergence is gauged by changing the mesh. While

TABLE VI. IR counterterms required by graphs 1–28.

Graph	Counterterm	Graph	Counterterm
4	$-C$	13	$2D+B$
5	$-D$	18	C
6	$-A$	21	D
7	$-B$	22	$-C$
9	$-C$	23	$-D$
10	$-D$	25	$-\frac{1}{2}A$
12	$2C+A$	26	$\frac{1}{2}A$

some graphs are less well behaved than others, we are typically able to get accuracies of about $0.01(a/\pi)^3$. It is not unusual to use over 10^7 points on a graph.

Gaussian integration appears to be superior for the 5-dimensional integrals; however, for the higher-dimensional integrals the situation is not so clear. The Sheppey routine gives an "automatic" error estimate whereas the errors we have quoted using Gaussian integration are "eyeball" estimates—in most cases quite conservative ones. The results of De Rújula *et al.*[14] on graphs 1–3 were obtained using RIWIAD.[26] As analytic results are known for graph 2, a direct comparison is possible. Table III shows their error—although small—to be 4 times their estimated 90% confidence limit, which suggests that RIWIAD error estimates may be too small in some cases.

Our results for the graphs with analytic answers are in excellent agreement. We do not expect quite such good results for the higher-dimensional integrations.

Due to the limited number of integration points that can be used, there is a slight chance of a large error when using Gaussian integration. In fact, the difference between the present answer and our previously published result[1] is almost entirely due to an 8% error in one graph. To a considerable extent we have removed this kind of error by reintegrating all the graphs with a change of integration variables. The necessity for high accuracy is easily seen by noticing that the value of a typical one of the 28 numbers in Table III is greater than the sum of all 28 graphs. We have also integrated the absolute value of the integrand for each graph. These numbers are typically as large as the largest number in Table III, indicating large internal cancellations within each graph, which intensifies the problem of reducing the numerical error.

---

*Work supported in part by the U. S. Atomic Energy Commission under Contract No. AEC AT(30-1) 882.

†Work supported in part by the National Science Foundation under Grant No. NSF GP 25303.

[1]M. J. Levine and J. Wright, Phys. Rev. Lett. 26, 1351 (1971).

[2]M. J. Levine and J. Wright, *Colloquium on Advanced Computing Methods in Theoretical Physics* (Centre de Physique Théorique, Marseille, 1971).

[3]J. Schwinger, Proc. Nat. Acad. Sci. 37, 452 (1951); 37, 455 (1951); Phys. Rev. 73, 416 (1948); 76, 790 (1949).

[4]R. Karplus and N. M. Kroll, Phys. Rev. 77, 536 (1950). Errors in this paper were corrected in Ref. 5.

[5]A. Peterman, Helv. Phys. Acta 30, 407 (1957); C. M. Sommerfield, Ann. Phys. (N.Y.) 5, 26 (1958); M. V. Terent'ev, Zh. Eksp. Teor. Fiz. 43, 619 (1962) [Sov. Phys.—JETP 16, 444 (1963)].

[6]S. Brodsky and T. Kinoshita, Phys. Rev. D 3, 356 (1971).

[7]J. Calmet and M. Perrottet, Phys. Rev. D 3, 3101 (1971).

[8]J. Aldins, S. Brodsky, A. Dufner, and T. Kinoshita, Phys. Rev. D 1, 2378 (1970).

[9]J. A. Mignaco and E. Remiddi, Nuovo Cimento 60A, 519 (1969).

[10]C. Chang and M. Levine, private communication.

[11]S. Barbieri, M. Caffo, and E. Remiddi, Nuovo Cimento Lett. 5, 769 (1972).

[12]D. Billi, M. Caffo, and E. Remiddi, Nuovo Cimento Lett. 4, 657 (1972).

[13]J. Calmet and A. Peterman, CERN Report No. CERN-TH-1724, 1973 (unpublished).

[14]A. De Rújula, B. Lautrup, and A. Peterman, Phys. Lett. 33B, 605 (1970).

[15]M. Levine and R. Roskies, Phys. Rev. Lett. 30, 772 (1973); Phys. Rev. D (to be published).

[16]T. Kinoshita and P. Cvitanovic, Phys. Rev. Lett. 29, 1534 (1972).

[17]Raymond Carroll and York-Peng Yao, Univ. of Michigan Report No. HE 73 19 (unpublished).

[18]J. C. Wesley and A. Rich, Phys. Rev. A 4, 1341 (1971). S. Granger and G. Wilford [Phys. Rev. Lett. 28, 1479 (1972)] have applied a correction to the Wesley-Rich number of 1 159 657.7 to obtain 1 159 656.7.

[19]B. E. Lautrup, A. Peterman, and E. deRafael, Phys. Rep. 3C, 193 (1972).

[20]S. J. Brodsky and Sidney D. Drell, Annu. Rev. Nucl. Sci. 20, 147 (1970).

[21]B. N. Taylor, W. Parker, and D. N. Langenberg, Rev. Mod. Phys. 41, 375 (1969).

[22]S. J. Brodsky and R. Roskies, Phys. Lett. 41B, 517 (1972); S. J. Brodsky, R. Roskies, and R. Suaya, to be published.

[23]J. S. R. Chisholm, Proc. Camb. Philos. Soc. 48, 300 (1952).

[24]M. J. Levine, AEC Report No. CAR-882-25, 1971 (unpublished); J. Comput. Phys. 1, 454 (1967).

[25]D. R. Yennie, S. C. Frautschi, and H. Suura, Ann. Phys. (N.Y.) 13, 379 (1961).

[26]G. C. Sheppey, private communication. Modifications of this program exist under the names LSD, SPCINT, RIWIAD used in W. Czyż, G. C. Sheppey, and J. D. Walecka, Nuovo Cimento 39, 420 (1964).